Current Biology 21, 1593–1602, October 11, 2011 ©2011 Elsevier Ltd All rights reserved DOI 10.1016/j.cub.2011.08.028

Article

In Vivo Optogenetic Stimulation of Neocortical Excitatory Neurons Drives Brain-State-Dependent Inhibition

Celine Mateo,[1,2] Michael Avermann,[1,3] Luc J. Gentet,[1] Feng Zhang,[4,5] Karl Deisseroth,[4] and Carl C.H. Petersen[1,*]
[1]Laboratory of Sensory Processing, Brain Mind Institute, Faculty of Life Sciences, École Polytechnique Fédérale de Lausanne (EPFL), CH-1015 Lausanne, Switzerland
[2]Department of Physics, University of California, San Diego, La Jolla, CA 92093, USA
[3]Friedrich Miescher Institute for Biomedical Research, 4058 Basel, Switzerland
[4]Department of Bioengineering, Stanford University, Stanford, CA 94305, USA
[5]Department of Brain and Cognitive Sciences, Massachusetts Institute of Technology, Cambridge, MA 02139-4307, USA

Summary

Background: Synaptic interactions between excitatory and inhibitory neocortical neurons are important for mammalian sensory perception. Synaptic transmission between identified neurons within neocortical microcircuits has mainly been studied in brain slice preparations in vitro. Here, we investigate brain-state-dependent neocortical synaptic interactions in vivo by combining the specificity of optogenetic stimulation with the precision of whole-cell recordings from postsynaptic excitatory glutamatergic neurons and GFP-labeled inhibitory GABAergic neurons targeted through two-photon microscopy.
Results: Channelrhodopsin-2 (ChR2) stimulation of excitatory layer 2/3 barrel cortex neurons evoked larger and faster depolarizing postsynaptic potentials and more synaptically driven action potentials in fast-spiking (FS) GABAergic neurons compared to both non-fast-spiking (NFS) GABAergic neurons and postsynaptic excitatory pyramidal neurons located within the same neocortical microcircuit. The number of action potentials evoked in ChR2-expressing neurons showed low trial-to-trial variability, but postsynaptic responses varied strongly with near-linear dependence upon spontaneously driven changes in prestimulus membrane potential. Postsynaptic responses in excitatory neurons had reversal potentials, which were hyperpolarized relative to action potential threshold and were therefore inhibitory. Reversal potentials measured in postsynaptic GABAergic neurons were close to action potential threshold. Postsynaptic inhibitory neurons preferentially fired synaptically driven action potentials from spontaneously depolarized network states, with stronger state-dependent modulation in NFS GABAergic neurons compared to FS GABAergic neurons.
Conclusions: Inhibitory neurons appear to dominate neocortical microcircuit function, receiving stronger local excitatory synaptic input and firing more action potentials compared to excitatory neurons. In mouse layer 2/3 barrel cortex, we propose that strong state-dependent recruitment of inhibitory neurons drives competition among excitatory neurons enforcing sparse coding.

*Correspondence: carl.petersen@epfl.ch

Introduction

Computations in cortical circuits underlie important aspects of mammalian sensory perception, associative learning, and cognition. A causal and mechanistic understanding of cortical function must consider synaptic interactions within local neocortical microcircuits composed of excitatory and inhibitory neurons. The vast majority of cortical neurons are excitatory and release glutamate, evoking small-amplitude unitary excitatory postsynaptic potentials (uEPSPs) in synaptically coupled target neurons. Although inhibitory GABAergic neocortical neurons account for only ~15% of the neuronal population, they are thought to play a key role in organizing neocortical network activity. Among the strongest synaptically coupled classes of neurons studied in vitro are the interactions between excitatory and inhibitory neurons [1–11], presumably reflecting a basic need to balance excitation and inhibition within the neocortex [12–16]. However, little is currently known about the synaptic interactions driving neocortical microcircuit dynamics in vivo, which are likely to be profoundly affected by spontaneous activity in a brain-state-dependent manner [16–23]. Here, we therefore combine optogenetic channelrhodopsin-2 (ChR2) [24, 25] stimulation of excitatory layer 2/3 pyramidal neurons with in vivo whole-cell membrane potential recordings to define cell-type-specific and brain-state-dependent synaptic interactions within layer 2/3 of the C2 barrel column of mouse primary somatosensory neocortex [26].

Results

Lentivirus-Mediated Expression of ChR2 in Excitatory Layer 2/3 Pyramidal Neurons of the Mouse C2 Barrel Column

Lentivirus encoding ChR2-YFP under the control of the αCaMKII promoter [27] was injected into layer 2/3 of the C2 barrel column, identified through intrinsic signal optical imaging (Figure 1A). Lentivirus preferentially infects excitatory neurons compared to inhibitory neurons in the mouse somatosensory neocortex [28]. The native αCaMKII promoter drives expression in only a part of the population of neocortical excitatory neurons [29], and it is therefore possible that our viral construct expresses preferentially in a subset of excitatory neurons. Lentivirus transduced cells with somata located near the injection site (full-width mean ± standard deviation [SD]: horizontal 144 ± 38 μm; vertical 292 ± 75 μm; n = 6), and it did not transduce neurons in other regions with axons projecting to the injection site [30]. Layer 2/3 of the mouse C2 barrel column has a horizontal diameter of ~250 μm and a vertical extent of ~300 μm, containing ~1,700 excitatory neurons [31]. There are therefore ~500 neurons within the spatial extent of the cortex transduced by our lentiviral injections. Following several weeks of expression, ChR2-YFP fluorescence can be imaged in vivo confirming local and correct targeting to layer 2/3 pyramidal neurons of the C2 barrel column (Figure 1B). Optogenetic stimulation of these localized layer 2/3 ChR2-expressing neurons did not evoke whisker movements in awake head-restrained mice, unlike blue light

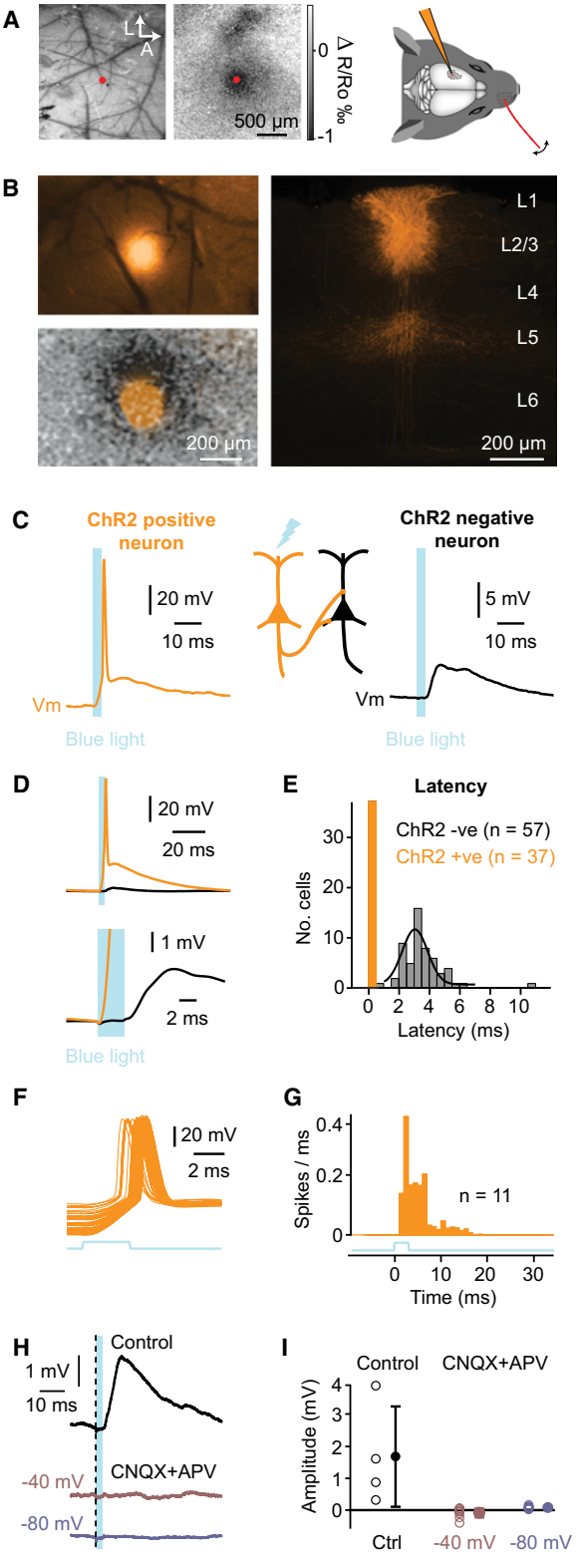

Figure 1. Optogenetic Stimulation of Excitatory Layer 2/3 Pyramidal Neurons of the Mouse C2 Barrel Column

(A) Lentivirus encoding ChR2-YFP under the control of the αCaMKII promoter was injected into the C2 barrel column localized using intrinsic signal optical imaging.

(B) In vivo epifluorescence of ChR2-YFP expression (upper left) is localized to the C2 column mapped by intrinsic signal optical imaging (lower left). ChR2-YFP expressing neurons are localized to layer 2/3 (fixed coronal section, right). Note the prominent axonal projection to layer 5.

(C) Optogenetic stimulation evoked depolarizing responses with shorter latency in ChR2-expressing neurons (orange) compared to ChR2-non-expressing postsynaptic neurons (black).

(D) Overlay and zoom of the same example light-evoked responses.

(E) Histogram of depolarization onset latencies of layer 2/3 excitatory neurons.

(F) Light-evoked action potential firing in ChR2-expressing neurons was reliable across trials (60 consecutive trials from the same recording are superimposed).

(G) Peristimulus time histogram (PSTH) of light-evoked action potential firing in ChR2-expressing neurons.

(H) The postsynaptic optogenetic response was blocked by surface application of CNQX and APV.

(I) CNQX and APV robustly blocked the postsynaptic light-evoked response at both depolarized (−40 mV) and hyperpolarized (−80 mV) membrane potentials. Each open circle represents an individual neuron. Filled circles with error bars represent mean ± standard deviation (SD).

stimulation of primary somatosensory barrel cortex of Thy1-ChR2 transgenic mice (see Figure S1 available online) [32].

Functional Characterization of the Optogenetic Stimulus through In Vivo Whole-Cell Membrane Potential Recordings

In order to measure the neocortical response evoked by optogenetic stimulation, we targeted in vivo whole-cell recordings to the injection site, recording from excitatory layer 2/3 pyramidal neurons in urethane anesthetized mice (and, in a smaller number of experiments, in awake head-restrained mice). Brief blue light flashes (3 ms, ~10 mW/mm^2) generated by a LED at 1 Hz evoked two different types of responses in recorded neurons (Figures 1C and 1D). In one class of neurons (37 out of 94 neurons), light evoked a depolarizing response, which began almost immediately after the onset of the light stimulus with a latency of 0.22 ± 0.05 ms (n = 37) (Figure 1E). These short latency neurons presumably express ChR2, allowing them to be directly depolarized by the light-activated ChR2 cation channel. Out of the 25 ChR2-expressing neurons from which we obtained stable long-lasting recordings, only 11 fired action potentials (APs) in response to our light stimulus, but they did so reliably (Figures 1F and 1G; Figure S1). The first spike latency was 3.5 ± 1.4 ms (n = 11), and the spike time jitter in individual ChR2-expressing neurons was low (SD of spike time: 0.36 ± 0.26 ms; n = 11). Across the recorded ChR2-expressing neurons that fired action potentials, 70% of the evoked spikes occurred within 5 ms of the onset of the light stimulus, and 92% occurred within 10 ms of the onset of the light stimulus (Figure 1G; Figure S1).

We estimate that our average lentiviral injection site contains ~500 neurons of which ~39% (37 out of 94) express ChR2. Approximately 44% (11 out of 25) of these ChR2-expressing neurons fire light-evoked action potentials in response to our 3 ms light stimulus. In our experiments, we estimate that ~100 excitatory ChR2-expressing neurons (500 × 0.39 × 0.44 = 86 neurons) will respond with light-evoked action potential firing forming the optogenetic excitatory presynaptic stimulus in our experiments.

The second class of excitatory neurons (57 out of 94 neurons) also depolarized in response to the 3 ms blue light flashes (amplitude 2.1 ± 2.2 mV; full width at half-maximal duration 14 ± 11 ms; n = 42) but with much longer latencies of 3.5 ± 1.5 ms (n = 57) (Figures 1C–1E). This class of long latency depolarizing neurons presumably corresponds to cells not expressing ChR2 but receiving subthreshold synaptic

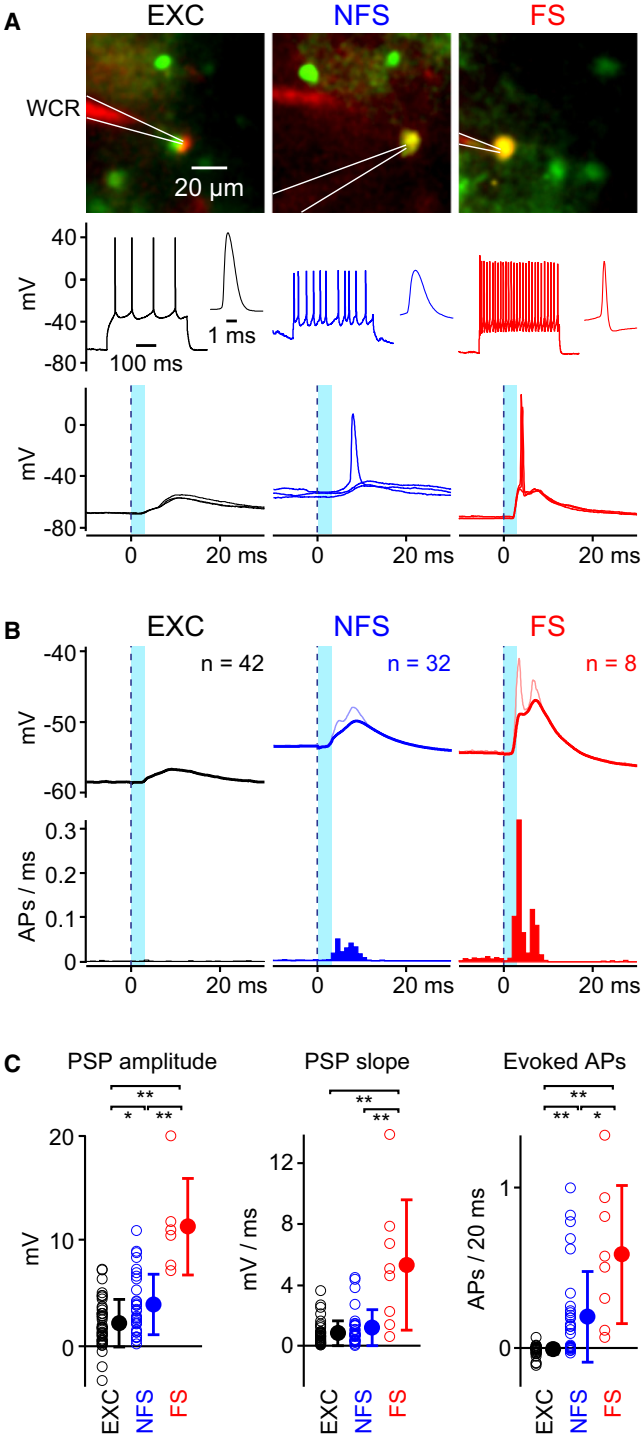

Figure 2. Cell-Type-Specific Postsynaptic Responses Evoked by Optogenetic Stimulation

(A) Whole-cell recordings (WCR, red fluorescence) were targeted to GFP-expressing fast-spiking (FS) and non-fast-spiking (NFS) GABAergic neurons and non-GFP-expressing excitatory (EXC) neurons in GAD67-GFP mice. All three neurons were recorded in the same mouse with somata located within 100 μm of each other.

(B) Grand average membrane potential traces (thick traces show Vm averaged with action potentials truncated at threshold; thin traces show raw Vm average; upper) and action potential PSTHs (1 ms bin, lower) across all recordings of postsynaptic neurons, averaged with respect to the same cell type.

(C) Postsynaptic potential (PSP) amplitude, PSP slope (rate of rise of initial 20%–50% response), and evoked firing (difference in action potential number comparing the 20 ms after optogenetic stimulus with the preceding 20 ms). Each open circle represents an individual neuron. Filled circles with error bars represent mean ± SD. Statistical significance is *$p < 0.017$, **$p < 0.0017$.

input driven by action potential activity in nearby ChR2-expressing neurons.

In order to establish the postsynaptic nature of those long latency responses, we applied antagonists of ionotropic glutamate receptors. Surface application of CNQX and APV (to block AMPA and NMDA receptors, respectively) completely suppressed the optogenetically evoked postsynaptic response, both at hyperpolarized and depolarized potentials (Figures 1H and 1I). Quantified across four mice, the amplitude of the light-evoked postsynaptic potential (PSP) before drug application was 1.7 ± 1.6 mV, which was reduced to 0.09 ± 0.04 mV after application of CNQX and APV (measured at resting membrane potential, n = 9 recordings). When the postsynaptic neuron was depolarized by current injection to −40 mV in the presence of CNQX and APV, the light-evoked PSP amplitude was −0.08 ± 0.15 mV (n = 9 recordings). These pharmacological manipulations show that the postsynaptic responses are entirely dependent upon glutamatergic synaptic transmission, confirming that the optogenetic stimulus is functionally targeted to excitatory neurons.

Cell-Type-Specific Postsynaptic Responses

In vitro studies have generally found that the local synaptic output from excitatory neocortical neurons is stronger onto GABAergic neurons compared to excitatory neurons [3–6, 11]. In order to investigate postsynaptic cell-type specificity in vivo, we used two-photon microscopy to target whole-cell recordings to fluorescently labeled GABAergic neurons in GAD67-GFP mice (Figure 2A) [16, 33]. We separated GABAergic neurons into two classes based on action potential waveform. Fast-spiking (FS) GABAergic neurons had action potential duration of under 0.5 ms (measured at half-maximal amplitude from threshold) and were able to fire action potentials at high rates with little accommodation, whereas non-fast-spiking (NFS) GABAergic neurons had action potentials with a duration of longer than 0.5 ms and had adapting firing patterns (Figure 2A). GABAergic neurons on average were depolarized compared to excitatory neurons (FS, −54.5 ± 6.1 mV, n = 8; NFS, −53.4 ± 4.9 mV, n = 32; EXC, −58.6 ± 7.3 mV, n = 42) (Figure S2). GABAergic FS neurons spontaneously fired action potentials at a higher rate than NFS GABAergic neurons and excitatory neurons (FS, 6.6 ± 5.6 Hz, n = 8; NFS, 1.4 ± 1.7 Hz, n = 32; EXC, 0.79 ± 0.92 Hz, n = 42) (Figure S2).

The postsynaptic responses evoked by the optogenetic stimulus were significantly different in each of the three classes of layer 2/3 neurons. FS GABAergic neurons had the largest amplitude depolarizing PSPs (FS, 11.3 ± 4.6 mV, n = 6; NFS, 3.9 ± 2.8 mV, n = 31; EXC, 2.1 ± 2.2 mV, n = 42) with the largest initial PSP slopes (FS, 5.3 ± 4.3 mV/ms, n = 8; NFS, 1.2 ± 1.2 mV/ms, n = 30; EXC, 0.87 ± 0.79 mV/ms, n = 38) (Figures 2B and 2C). Postsynaptic FS GABAergic neurons also fired more action potentials in response to the optogenetic stimulus compared to postsynaptic NFS GABAergic neurons or excitatory neurons (change in action potential firing comparing 20 ms after light stimulus with 20 ms before light stimulus: FS, 0.58 ± 0.43 APs, n = 8; NFS, 0.19 ± 0.28 APs, n = 32;

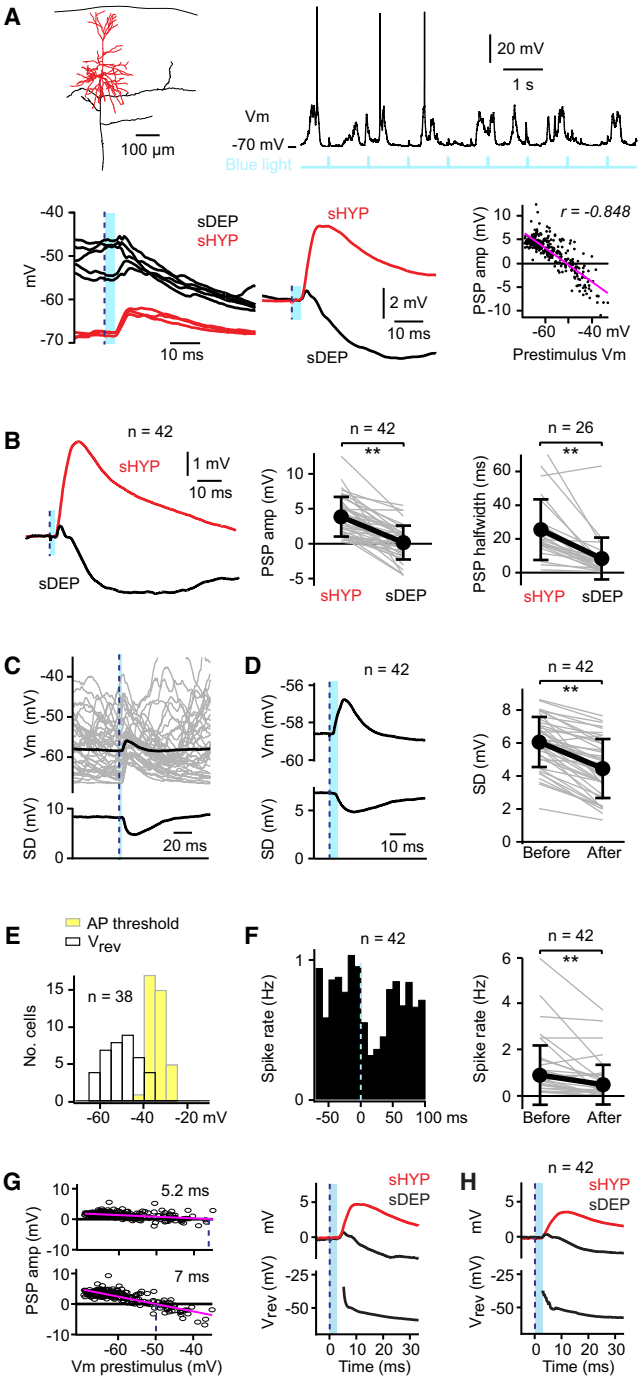

Figure 3. The Optogenetic Stimulus Inhibits Postsynaptic Excitatory Layer 2/3 Neurons

(A) Light-evoked PSPs recorded in a postsynaptic layer 2/3 pyramidal neuron were larger when delivered during spontaneously hyperpolarized states (sHYP, red) compared to periods of spontaneously depolarized network activity (sDEP, black) (lower left and lower center). The PSP amplitude (quantified at the peak time of the average PSP) was near-linearly correlated to prestimulus membrane potential (lower right).

(B) Quantified across all recordings from postsynaptic excitatory neurons, the PSP amplitude and duration were significantly smaller in the sDEP state.

(C) Optogenetic stimulation reduced membrane potential SD computed across trials (example experiment).

(D) Quantified across all recordings, the optogenetic stimulus significantly reduced membrane potential variance.

(E) The spontaneously driven reversal potentials of the light-evoked PSPs were hyperpolarized relative to action potential threshold for each recorded neuron.

(F) Optogenetic stimulation significantly decreases the firing rate in excitatory postsynaptic cells (left), quantified for each individual neuron comparing 50 ms before and 50 ms after the light stimulus (right).

(G) An example experiment showing the reversal potential computed for different times after onset of the blue light stimulus (reversal potential at 5.2 ms was −34 mV, and at 7 ms it was −50 mV).

(H) The time-dependent reversal potential of the optogenetically evoked PSP computed across all postsynaptic excitatory neurons.

Each gray line represents an individual neuron. Black circles with error bars represent mean ± SD. Statistical significance is **p < 0.005.

EXC, −0.011 ± 0.03 APs, n = 42) (Figures 2B and 2C). The latency for evoking postsynaptic action potentials following light onset was short in both FS and NFS GABAergic neurons (FS, 4.5 ± 1.5 ms, n = 8; NFS, 6.5 ± 1.7 ms, n = 24), with FS neurons firing significantly earlier (p = 0.004).

Spontaneous Cortical Activity Does Not Affect Light-Evoked Action Potential Firing in ChR2-Expressing Neurons under Our Experimental Conditions

Neocortical microcircuits in vivo are spontaneously active with large-amplitude membrane potential fluctuations that are highly correlated in nearby neurons (Figure S2) [15–17, 21, 34, 35]. This internally generated spontaneous activity interacts strongly with sensory processing, suppressing the sensory response in the barrel cortex evoked by a single brief whisker deflection [17, 18]. It is therefore of critical importance to examine the interaction of the ChR2 stimulus with spontaneous activity in the neocortical microcircuit.

We first analyzed the effects of spontaneous membrane potential changes upon the ChR2-expressing neurons, finding that under our experimental conditions, spontaneous activity made little impact upon the direct light-evoked spiking responses. We distinguished between spontaneous depolarized (sDEP) and hyperpolarized states (sHYP) of the local neocortical neuronal network. Comparing across trials, we found that action potentials were evoked by the light stimulus with equal probabilities from spontaneously hyperpolarized and spontaneously depolarized states of cortical network activity (quantified over the 10 ms following onset of blue light stimulus: sHYP 0.66 ± 0.86 spikes; sDEP 0.69 ± 0.89 spikes; n = 25) (Figure S1). Under our experimental conditions, the number of light-evoked action potentials in ChR2-expressing neurons is therefore independent of spontaneous cortical activity, providing a reliable and well-defined optogenetic stimulation of presynaptic layer 2/3 pyramidal neurons.

Highly Variable Light-Evoked Postsynaptic Membrane Potential Changes

Because the optogenetic presynaptic stimulus was reliable across trials, we were surprised to find highly variable postsynaptic responses. The postsynaptic responses in ChR2-nonexpressing excitatory pyramidal neurons were depolarizing in some trials but hyperpolarizing in other trials (Figure 3A). A large part of the variability could be accounted for by considering the prestimulus membrane potential. In trials where the light stimulus occurred during the spontaneously hyperpolarized state (sHYP) of the local neocortical microcircuit, the postsynaptic response was a large-amplitude, relatively long-lasting depolarization (PSP amplitude measured at the peak of the average response: 3.8 ± 2.8 mV, n = 42; full width at half maximal amplitude PSP

duration: 25.5 ± 18.0 ms, n = 26) (Figures 3A and 3B). However, in trials when the light-evoked stimulus occurred during a spontaneously depolarized (sDEP) period of cortical network activity, the postsynaptic response was either hyperpolarizing or had only a brief small-amplitude depolarization (PSP amplitude: 0.1 ± 2.4 mV, n = 42; PSP duration: 8.4 ± 12.5 ms, n = 26) (Figure 3A and 3B). Plotting the amplitude of the evoked PSP (measured at the peak time of the averaged response) as a function of the prestimulus membrane potential revealed a close to linear relationship, which was significant in 38 out of 42 recordings ($p < 0.01$; correlation coefficient −0.72 ± 0.19, n = 38). The optogenetic stimulus reduced membrane potential variance (Figures 3C and 3D) by driving the postsynaptic membrane potential toward a reversal potential, perhaps forming an underlying mechanism contributing to other stimulus-induced reductions in neural variability [36]. The PSP reversal potential (−50.2 ± 7.0 mV, n = 38; measured at the peak time of the averaged response) was hyperpolarized relative to action potential threshold (−34.0 ± 3.6 mV, n = 38) for each postsynaptic excitatory neuron (Figure 3E). As a consequence, the spiking rate in postsynaptic excitatory neurons was significantly decreased by the optogenetic light stimulation of ChR2-expressing presynaptic excitatory layer 2/3 pyramidal neurons (50 ms before the stimulation: 0.91 ± 1.28 Hz; 50 ms after the stimulation: 0.50 ± 0.86 Hz; n = 42; $p < 0.001$) (Figure 3F). The overall decrease in firing in postsynaptic excitatory neurons was also significant when computed over a 20 ms timescale (20 ms before the stimulation: 1.0 ± 1.7 Hz; 20 ms after the stimulation: 0.44 ± 0.78 Hz; n = 42; $p < 0.005$) but not over a 10 ms timescale (10 ms before the stimulation: 0.96 ± 1.68 Hz; 10 ms after the stimulation: 0.55 ± 1.0 Hz; n = 42; $p = 0.31$). Two postsynaptic excitatory neurons fired with slightly increased probability, which was significant when evaluated within 10 ms of the optogenetic stimulus (the difference in the number of action potentials comparing 10 ms after stimulus onset with 10 ms before stimulus onset: 0.026 evoked spikes for cell #114, $p = 0.034$; 0.017 evoked spikes for cell #111, $p = 0.028$), but this increase was not significant when quantified over longer timescales (the difference in the number of action potentials comparing 20 ms after stimulus onset with 20 ms before stimulus onset: 0.011 evoked spikes for cell #114, $p = 0.41$; −0.0013 evoked spikes for cell #111; $p = 0.88$). Interestingly, these two neurons received the two fastest-rising PSPs out of the 42 recorded postsynaptic excitatory neurons.

When analyzed at different times after the optogenetic stimulus, the reversal potentials indicated a larger contribution of excitatory conductances for a brief period of a few milliseconds during the rising phase of the depolarizing postsynaptic potential (Figures 3G and 3H). Across all recordings with significant correlations at the quantified time point, we found that at 5 ms after the onset of blue light, the reversal potential was −45.6 ± 12.0 mV (n = 23), whereas a few milliseconds later at 10 ms, the reversal potential was −52.1 ± 7.1 mV (n = 37). The optogenetic stimulus therefore evokes rapid excitation, which is almost immediately quenched by inhibition.

The overall inhibitory effect upon surrounding postsynaptic excitatory neurons evoked by the optogenetic stimulus was robust, being observed in both anesthetized and awake recordings (comparing 50 ms after optogenetic stimulation with 50 ms before optogenetic stimulation, the firing rate in postsynaptic excitatory neurons in awake recordings was reduced by 52%, $p = 0.008$, and in anesthetized recordings it was reduced by 44%, $p = 0.0006$) (Figure S3).

In agreement with Waters and Helmchen [37], we did not find changes in somatic input resistance during spontaneous activity, which under other experimental conditions could contribute to response differences [38]. Input resistance measured at the soma was 64.9 ± 22.7 MΩ during sHYP states and 64.1 ± 21.2 MΩ during sDEP states (n = 12) (Figure S4).

GABAergic Neurons Fire Light-Evoked Synaptically Driven Action Potentials Preferentially during Periods of Spontaneously Depolarized Cortical Network Activity

Analyses of the state dependence of the reversal potential during current injections suggested that inhibitory conductances were stronger when optogenetic stimuli were delivered during sDEP periods compared to sHYP periods (Figure S4). In order to directly examine the cell-type-specificity and the state dependence of the recruitment of GABAergic inhibitory neurons, we investigated trial-by-trial variability of postsynaptic responses in our recordings from GFP-labeled GABAergic neurons. Analyzing light-evoked responses separately for sHYP and sDEP states revealed that inhibitory GABAergic neurons preferentially fired light-evoked action potentials during spontaneously depolarized periods of network activity (quantified over the 20 ms following blue light onset, with spontaneous firing subtracted: sDEP 0.42 ± 0.40 evoked spikes per stimulus; sHYP 0.17 ± 0.34 evoked spikes per stimulus; n = 40). The preferential light-evoked spiking activity of postsynaptic GABAergic neurons during periods of depolarized spontaneous network activity therefore provides a clear mechanistic explanation for the prominent light-evoked hyperpolarizations evoked in postsynaptic pyramidal neurons during the sDEP cortical state.

Separating between NFS GABAergic neurons (Figure 4A) and FS GABAergic neurons (Figure 4B) revealed interesting cell-type-specific differences in suprathreshold responses. Optogenetic stimulation during sDEP states evoked substantial action potential firing in both NFS and FS GABAergic neurons, with approximately double the number of evoked spikes in FS GABAergic neurons (during sDEP states, the difference in action potential firing comparing trials with and without light stimuli: FS, 0.74 ± 0.24 evoked spikes per stimulus within 20 ms, n = 8; NFS, 0.34 ± 0.40 evoked spikes per stimulus within 20 ms, n = 32) (Figure 4C; Figure 6B). FS GABAergic neurons occasionally fired doublets of action potentials in response to the optogenetic stimulus, but this was never observed in NFS GABAergic neurons. During sHYP states the optogenetic stimulus evoked fewer action potentials in both FS and NFS GABAergic neurons. During sHYP states, FS GABAergic neurons fired approximately four times the number of evoked action potentials compared to NFS GABAergic neurons (during sHYP states, the difference in action potential firing comparing trials with and without light stimuli: FS, 0.42 ± 0.53 evoked spikes per stimulus within 20 ms, n = 8; NFS, 0.11 ± 0.26 evoked spikes per stimulus within 20 ms, n = 32) (Figure 4C; Figure 6B). Whereas FS GABAergic neurons are the major class of inhibitory neurons recruited by the optogenetic stimulus during sHYP states, NFS GABAergic neurons also contribute substantially during sDEP states.

GABAergic neurons clearly behave very differently from excitatory neurons in terms of evoked postsynaptic action potential firing. We therefore wondered whether there might be differences in how the optogenetically evoked synaptic inputs are integrated in excitatory and inhibitory neurons. Analyzing trials in which no action potentials were evoked in the recorded postsynaptic neuron, we found that the PSP amplitude in both NFS GABAergic neurons (Figure 5A;

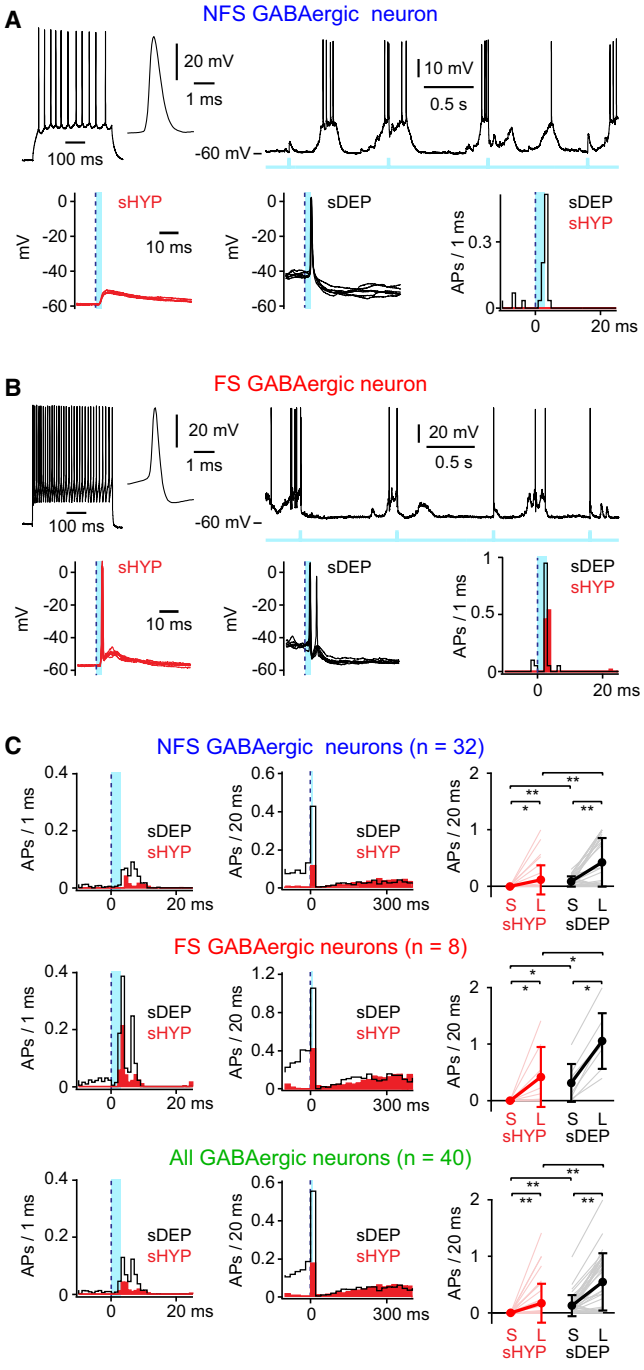

Figure 4. The Optogenetic Stimulus Synaptically Drives State-Dependent Action Potential Firing in GABAergic Neurons

(A) In an example NFS GABAergic neuron, optogenetic stimuli evoked subthreshold depolarization during sHYP (red), but evoked action potential firing during sDEP (black).

(B) The optogenetic stimulus reliably evoked action potentials in both sHYP and sDEP states in this example FS GABAergic neuron. In the sDEP state, doublets of action potentials were occasionally evoked.

(C) PSTHs of action potential firing computed across all recordings of NFS GABAergic neurons (upper), FS GABAergic neurons (middle), and all GABAergic neurons (lower). The PSTHs are shown at high temporal resolution (left) around the time of the optogenetic stimulus and the same PSTHs are also shown over a longer time scale (middle). Quantification of action potential firing in each neuron (right) over 20 ms periods of spontaneous activity (labeled "S" for spontaneous) is compared with the 20 ms periods following the optogenetic stimulus (labeled "L" for light stimulus). Each pink and gray line represents an individual neuron. Red and black circles with error bars represent mean ± SD. Statistical significance is *$p < 0.05$, **$p < 0.005$.

Figure 6A) and FS GABAergic neurons (Figure 5B; Figure 6A) were affected relatively little by spontaneous cortical activity compared to the dramatic reduction in PSP amplitude observed in excitatory neurons during sDEP states (Figure 3; Figure 6A). PSP amplitude was significantly correlated with spontaneous prestimulus membrane potential in some FS and NFS neurons ($p < 0.01$ in four out of eight recordings of FS neurons, correlation coefficient -0.69 ± 0.05, $n = 4$; $p < 0.01$ in 20 out of 32 recordings from NFS neurons, correlation coefficient -0.54 ± 0.23, $n = 20$). The spontaneously driven reversal potential of the subthreshold PSPs was -36.6 ± 5.6 mV ($n = 4$) for FS GABAergic neurons and -39.0 ± 10.6 mV ($n = 20$) for NFS GABAergic neurons (Figure 5C; Figure 6C). The membrane potential of GABAergic neurons is therefore driven toward action potential threshold (FS GABAergic neurons -39.9 ± 2.2 mV, $n = 4$; NFS GABAergic neurons -38.8 ± 4.5 mV, $n = 20$) (Figure 5C; Figure 6C), providing a clear explanation for their suprathreshold responses to the optogenetic stimulus (Figure 4; Figure 6B).

Discussion

Through combining a precisely targeted optogenetic stimulation with in vivo whole-cell recordings, we probed the synaptic architecture of layer 2/3 microcircuits. Light-stimuli evoked reliable action potential firing in ~100 excitatory layer 2/3 neurons expressing ChR2. Surprisingly, the effect of the optogenetic stimulus was inhibitory on surrounding postsynaptic ChR2-non-expressing excitatory neurons, probably driven by state-dependent differential recruitment of FS and NFS GABAergic neurons.

Cell-Type-Specific Postsynaptic Responses

Optogenetic stimulation of excitatory layer 2/3 neurons evoked depolarization in all classes of recorded postsynaptic neurons within the same layer 2/3 microcircuit (Figure 7A). Interestingly, the strength of the postsynaptic depolarization varied across the different classes of layer 2/3 neurons, with a PSP amplitude ratio EXC:NFS:FS = 1:1.9:5.4 and a PSP slope ratio EXC:NFS:FS = 1:1.4:6.1. Synaptically driven postsynaptic action potentials were observed in GABAergic neurons, with FS GABAergic neurons firing 3.1 times more than NFS GABAergic neurons. Our in vivo measurements are consistent with previous in vitro measurements of synaptic connectivity, which report strong synaptic connectivity from excitatory neurons onto FS GABAergic neurons within local neocortical microcircuits [3, 11].

FS GABAergic neurons express parvalbumin [16, 39] and likely comprise both soma-targeting basket cells and axo-axonic cells [40, 41]. NFS GABAergic neurons do not express parvalbumin [16] and are likely to mainly consist of a variety of perisomatic- and dendrite-targeting neurons expressing other markers such as calretinin [16, 40, 41]. Parvalbumin-expressing FS GABAergic neurons with axons targeting soma or axon initial segment therefore appear to be the most active neurons in vivo within layer 2/3 mouse barrel cortex, receiving the largest excitatory synaptic input and firing the largest number of action potentials.

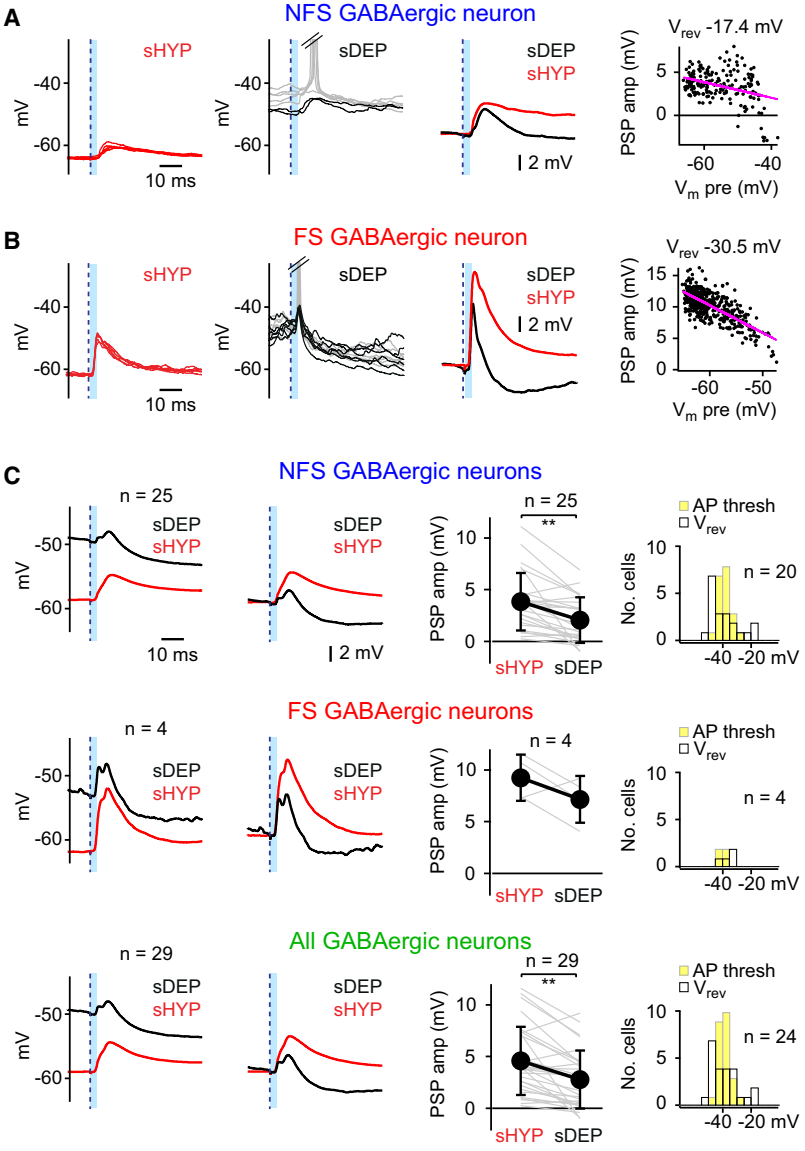

Figure 5. Depolarized Reversal Potential of Optogenetically Evoked Postsynaptic Response in GABAergic Neurons

(A) Spontaneous depolarization made little impact on the PSP amplitude in this example NFS GABAergic neuron.
(B) Same as (A), but for a FS GABAergic neuron.
(C) Grand average membrane potential traces across all recorded neurons including only trials without light-evoked spiking (far left and center left) for NFS GABAergic neurons (upper), FS GABAergic neurons (middle), and all GABAergic neurons (lower). PSP amplitude is reduced during sDEP states (center right) but to a much smaller extent than for excitatory neurons. The spontaneously driven PSP reversal potentials were similar to action potential thresholds (far right). Each gray line represents an individual neuron and black circles with error bars represent mean ± SD. Statistical significance is **$p < 0.005$.

State-Dependent Operation of the Neocortical Microcircuit

The postsynaptic responses evoked by our precise and reliable optogenetic stimulus were strongly influenced by spontaneous ongoing cortical activity (Figure 7B). The optogenetically evoked PSPs had a close to linear relationship with respect to prestimulus membrane potential. The PSP reversal potentials were hyperpolarized relative to action potential threshold for excitatory neurons but not for GABAergic neurons (Figure 6C). As a consequence, the optogenetic stimulation of presynaptic excitatory neurons had a net inhibitory effect on the spike output of postsynaptic excitatory neurons (Figure 3F). Interestingly, the optogenetic stimulus evoked action potential firing in GABAergic neurons preferentially from depolarized cortical states, with NFS GABAergic neurons showing the strongest state-dependent modulation.

The state-dependent recruitment of inhibition provides a mechanism to differentially balance excitation and inhibition. During periods of cortical inactivity, when the cortical microcircuit is hyperpolarized (sHYP), excitatory neurons can evoke long-lasting and large-amplitude PSPs. During sHYP periods, the neocortical microcircuits are therefore in a sensitive detection state ready to be activated over a relatively long integration window. However, during periods of cortical activation, when the neocortical microcircuit is depolarized (sDEP), stimulation of excitatory neurons evokes only a brief small-amplitude depolarization followed by hyperpolarization. The excitatory synaptic integration time is therefore reduced during the spontaneously depolarized cortical state. Summation of near-coincident, large-amplitude, and fast-rising excitatory synaptic inputs may therefore be necessary for driving action potentials in excitatory layer 2/3 neurons [16, 21]. The rare large-amplitude uEPSPs that are found in connectivity analyses of neocortical excitatory neuronal networks in vitro might play a profound role in driving postsynaptic spiking [31].

The near-linear dependence of the amplitude of the optogenetically evoked PSP with respect to prestimulus membrane potential accounts for a large part of the variance of the response. Interestingly, sensory responses in excitatory layer 2/3 barrel cortex neurons evoked by passive stimulation [17, 18] or active touch [35] have a similar near-linear dependence upon prestimulus membrane potential with reversal potentials in general, hyperpolarized with respect to action potential threshold. Thus, although our optogenetic stimulus is an artificial perturbation of the cortical activity, it appears to be informative for understanding the synaptic mechanisms underlying cortical sensory processing. However, it is important to note that many additional factors are likely to contribute to response variability including neuromodulators, long-range synaptic inputs, and high-frequency spontaneous network activity.

Competition among Excitatory Neurons Mediated by Disynaptic Inhibition Drives Sparse Coding

Curiously, the net effect of stimulating excitatory neurons upon the surrounding layer 2/3 neocortical microcircuit was inhibitory. Even during periods of spontaneous network depolarization (when the postsynaptic excitatory neurons were closer to action potential threshold), the excitatory optogenetic stimulus failed to drive action potentials in excitatory

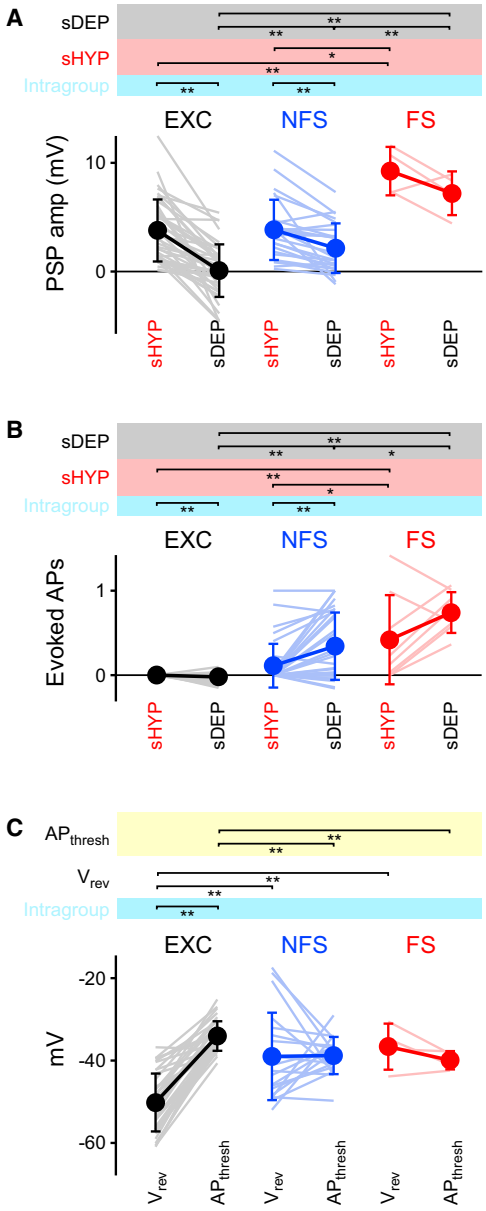

Figure 6. Cell-Type-Specific and Brain-State-Dependent Functional Architecture of the Neocortical Microcircuit In Vivo

(A) PSP amplitudes evoked by optogenetic stimulation across different cell types and cortical states.

(B) Postsynaptic action potential firing evoked by the optogenetic stimulus across different cell types and cortical states. Spontaneous action potential firing has been subtracted to derive the evoked response.

(C) PSP reversal potentials were hyperpolarized relative to action potential thresholds in excitatory neurons but not in GABAergic neurons.

Each lightly colored line represents an individual neuron. Circles with error bars represent mean ± SD. Statistical significance comparing across cell types is *$p < 0.017$, **$p < 0.0017$. Statistical significance comparing within a cell type is **$p < 0.005$.

postsynaptic neurons, instead evoking a hyperpolarizing response through disynaptic inhibition. Such circuit dynamics provide a mechanistic explanation for the sparse action potential activity of excitatory layer 2/3 pyramidal neurons [16, 19, 21, 42, 43], even during periods of active whisker sensing (median firing rates ~0.1 Hz, with ~10% of neurons contributing ~50% of total spikes) [35, 44]. Competition for action potential firing among layer 2/3 pyramidal neurons mediated by disynaptic inhibition may thus be an important feature of microcircuit function in layer 2/3 barrel cortex (Figure 7C). Conversely, because our optogenetic stimulus readily drives action potential firing in GABAergic neurons, our data account for the high firing rates observed for GABAergic neurons in vivo [16, 35, 42, 45–48].

Here, through combining optogenetics with in vivo whole-cell recordings, we have delineated basic operating principles of neocortical microcircuits. Our results reveal that the neocortical microcircuits have a state-dependent functional architecture, whereby depolarized states of the neocortex enable a robust recruitment of GABAergic neurons to balance excitation and inhibition. These in vivo microcircuit dynamics suggest that strong and rapid GABAergic inhibition mediates competition among excitatory layer 2/3 pyramidal neurons driving sparse coding.

Experimental Procedures

All experiments were carried out in accordance with the Swiss Federal Veterinary Office. C57BL6J and GAD67-GFP mice [33], 3–5 weeks old, were implanted with a lightweight metal head holder and a recording chamber under deep isoflurane anesthesia [16, 19, 21, 35]. The location of the left C2 barrel column was functionally located through intrinsic optical imaging under light isoflurane anesthesia [30]. A small volume (~50 nl) of lentivirus (10^7 IU/ml) encoding ChR2-YFP driven by the αCaMKII promoter [27] was injected into layer 2/3 of the C2 barrel column. In vivo whole-cell recordings were targeted to the injection site after allowing at least 4 weeks for expression of ChR2. Whole-cell membrane potential recordings were made in the C2 barrel column of mice under urethane anesthesia (1.7 mg/g) maintained at 37°C with a heating blanket. In addition, a small number of experiments were carried out in awake head-restrained mice. Patch pipettes (4–7 MΩ resistance) were filled with a solution containing (in mM): 135 potassium gluconate, 4 KCl, 10 HEPES, 10 Na_2Phosphocreatine, 4 MgATP, 0.3 Na_3GTP (adjusted to pH 7.3 with KOH), and 3 mg/ml biocytin for post hoc anatomical identification. For two-photon targeted recordings, 10 μM Alexa 594 (Invitrogen) was added to the pipette solution [16]. Whole-cell electrophysiological measurements were made with Multiclamp 700 amplifiers (Axon Instruments). The membrane potential was filtered at 10 kHz and digitized at 20 kHz by an ITC-18 (Instrutech Corporation) under the control of IgorPro (Wavemetrics). The membrane potential was not corrected for liquid junction potentials. Only cells in supragranular layers were analyzed (subpial depth < 450 μm). A superbright LED (Luxeon, Philips) generated blue light flashes, which were focused onto the cortex (3 ms, 1 Hz, 470 nm, ~10 mW/mm^2). All data are presented as mean ± SD. Nonparametric statistical tests (Wilcoxon-Mann-Whitney two-sample rank test or Wilcoxon Signed Rank test) were performed in IgorPro and used to assess significance, with Bonferroni correction for multiple comparisons.

Supplemental Information

Supplemental Information includes four figures and Supplemental Experimental Procedures and can be found with this article online at doi:10.1016/j.cub.2011.08.028.

Acknowledgments

We thank Rachel Aronoff, Julien Marquis, Vivianne Padrun, Fabienne Pidoux, and Jean-Charles Bensadoun for help with lentivirus production and Juan-Carlos Floyd Sarria for help with confocal imaging. We thank Aurelie Pala, Szabolcs Olah, Sylvain Crochet, and James Poulet for useful discussions and critical reading of an earlier version of the manuscript. This work was funded by grants from the Swiss National Science Foundation, Human Frontier Science Program, and SystemsX.ch.

Received: July 18, 2011
Revised: August 11, 2011
Accepted: August 11, 2011
Published online: September 22, 2011

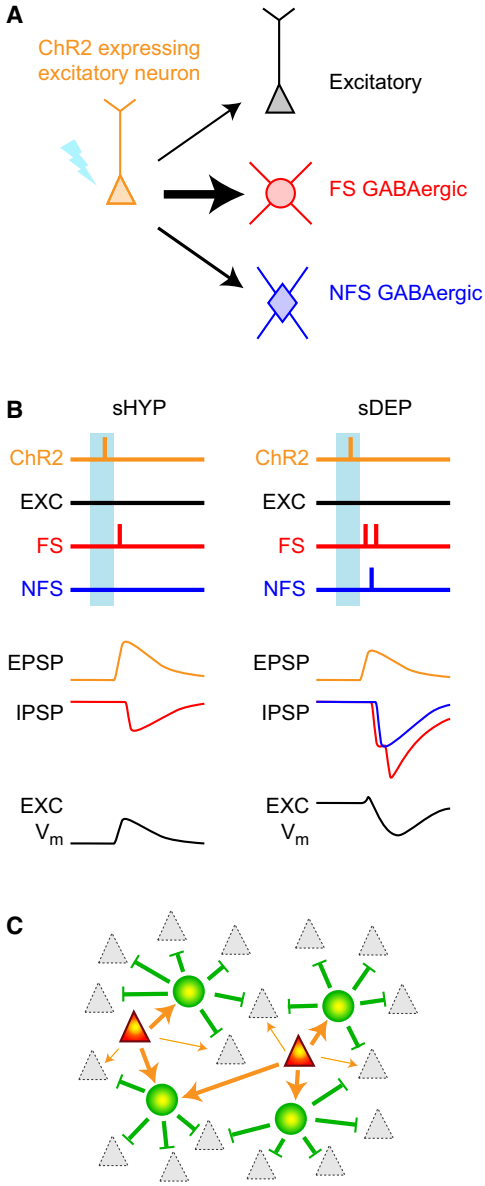

Figure 7. Schematic Summary

(A) Optogenetic stimulation of ChR2-expressing layer 2/3 pyramidal neurons evoked the largest excitatory synaptic input onto FS GABAergic neurons, with smaller input onto NFS GABAergic neurons and the least input onto postsynaptic excitatory neurons.

(B) The optogenetic stimulus evokes action potentials in ChR2-expressing excitatory neurons with the same probability in sDEP and sHYP cortical states. Postsynaptic FS GABAergic neurons are rapidly recruited to fire action potentials with more evoked spiking during sDEP states. NFS GABAergic neurons fire few action potentials from sHYP states but are recruited during sDEP states. The spontaneous differences in membrane potential alter the driving force for excitation, implying that postsynaptic excitatory neurons will receive larger excitatory postsynaptic potentials (EPSPs) during sHYP states compared to sDEP states. On the other hand, inhibition is enhanced during sDEP states both by the increased driving force for inhibitory postsynaptic potentials (IPSPs) and by the enhanced evoked action potential firing in GABAergic neurons. The synaptic integration of the state-dependent network activity evoked by the optogenetic stimulus drives long-lasting large-amplitude depolarization in postsynaptic excitatory neurons during sHYP states, but hyperpolarization dominates during sDEP states.

(C) Schematic illustration of optogenetically evoked action potential activity in ChR2-expressing excitatory neurons (orange) driving the efficient recruitment of inhibitory GABAergic neurons (green), which inhibit action potential firing in other nearby excitatory neurons (gray) of the local neuronal microcircuit. Strong disynaptic inhibition provides a mechanism for competition among layer 2/3 pyramidal neurons leading to sparse coding.

References

1. Reyes, A., Lujan, R., Rozov, A., Burnashev, N., Somogyi, P., and Sakmann, B. (1998). Target-cell-specific facilitation and depression in neocortical circuits. Nat. Neurosci. *1*, 279–285.
2. Gibson, J.R., Beierlein, M., and Connors, B.W. (1999). Two networks of electrically coupled inhibitory neurons in neocortex. Nature *402*, 75–79.
3. Holmgren, C., Harkany, T., Svennenfors, B., and Zilberter, Y. (2003). Pyramidal cell communication within local networks in layer 2/3 of rat neocortex. J. Physiol. *551*, 139–153.
4. Kapfer, C., Glickfeld, L.L., Atallah, B.V., and Scanziani, M. (2007). Supralinear increase of recurrent inhibition during sparse activity in the somatosensory cortex. Nat. Neurosci. *10*, 743–753.
5. Silberberg, G., and Markram, H. (2007). Disynaptic inhibition between neocortical pyramidal cells mediated by Martinotti cells. Neuron *53*, 735–746.
6. Helmstaedter, M., Staiger, J.F., Sakmann, B., and Feldmeyer, D. (2008). Efficient recruitment of layer 2/3 interneurons by layer 4 input in single columns of rat somatosensory cortex. J. Neurosci. *28*, 8273–8284.
7. Molnár, G., Oláh, S., Komlósi, G., Füle, M., Szabadics, J., Varga, C., Barzó, P., and Tamás, G. (2008). Complex events initiated by individual spikes in the human cerebral cortex. PLoS Biol. *6*, e222.
8. Pouille, F., Marin-Burgin, A., Adesnik, H., Atallah, B.V., and Scanziani, M. (2009). Input normalization by global feedforward inhibition expands cortical dynamic range. Nat. Neurosci. *12*, 1577–1585.
9. Xu, X., and Callaway, E.M. (2009). Laminar specificity of functional input to distinct types of inhibitory cortical neurons. J. Neurosci. *29*, 70–85.
10. Kätzel, D., Zemelman, B.V., Buetfering, C., Wölfel, M., and Miesenböck, G. (2011). The columnar and laminar organization of inhibitory connections to neocortical excitatory cells. Nat. Neurosci. *14*, 100–107.
11. Hofer, S.B., Ko, H., Pichler, B., Vogelstein, J., Ros, H., Zeng, H., Lein, E., Lesica, N.A., and Mrsic-Flogel, T.D. (2011). Differential connectivity and response dynamics of excitatory and inhibitory neurons in visual cortex. Nat. Neurosci. *14*, 1045–1052.
12. Borg-Graham, L.J., Monier, C., and Frégnac, Y. (1998). Visual input evokes transient and strong shunting inhibition in visual cortical neurons. Nature *393*, 369–373.
13. Wehr, M., and Zador, A.M. (2003). Balanced inhibition underlies tuning and sharpens spike timing in auditory cortex. Nature *426*, 442–446.
14. Wilent, W.B., and Contreras, D. (2005). Dynamics of excitation and inhibition underlying stimulus selectivity in rat somatosensory cortex. Nat. Neurosci. *8*, 1364–1370.
15. Okun, M., and Lampl, I. (2008). Instantaneous correlation of excitation and inhibition during ongoing and sensory-evoked activities. Nat. Neurosci. *11*, 535–537.
16. Gentet, L.J., Avermann, M., Matyas, F., Staiger, J.F., and Petersen, C.C.H. (2010). Membrane potential dynamics of GABAergic neurons in the barrel cortex of behaving mice. Neuron *65*, 422–435.
17. Petersen, C.C.H., Hahn, T.T.G., Mehta, M., Grinvald, A., and Sakmann, B. (2003). Interaction of sensory responses with spontaneous depolarization in layer 2/3 barrel cortex. Proc. Natl. Acad. Sci. USA *100*, 13638–13643.
18. Sachdev, R.N., Ebner, F.F., and Wilson, C.J. (2004). Effect of subthreshold up and down states on the whisker-evoked response in somatosensory cortex. J. Neurophysiol. *92*, 3511–3521.
19. Crochet, S., and Petersen, C.C.H. (2006). Correlating whisker behavior with membrane potential in barrel cortex of awake mice. Nat. Neurosci. *9*, 608–610.
20. Ferezou, I., Haiss, F., Gentet, L.J., Aronoff, R., Weber, B., and Petersen, C.C.H. (2007). Spatiotemporal dynamics of cortical sensorimotor integration in behaving mice. Neuron *56*, 907–923.
21. Poulet, J.F.A., and Petersen, C.C.H. (2008). Internal brain state regulates membrane potential synchrony in barrel cortex of behaving mice. Nature *454*, 881–885.
22. Haider, B., and McCormick, D.A. (2009). Rapid neocortical dynamics: Cellular and network mechanisms. Neuron *62*, 171–189.

23. Otazu, G.H., Tai, L.H., Yang, Y., and Zador, A.M. (2009). Engaging in an auditory task suppresses responses in auditory cortex. Nat. Neurosci. *12*, 646–654.
24. Nagel, G., Szellas, T., Huhn, W., Kateriya, S., Adeishvili, N., Berthold, P., Ollig, D., Hegemann, P., and Bamberg, E. (2003). Channelrhodopsin-2, a directly light-gated cation-selective membrane channel. Proc. Natl. Acad. Sci. USA *100*, 13940–13945.
25. Boyden, E.S., Zhang, F., Bamberg, E., Nagel, G., and Deisseroth, K. (2005). Millisecond-timescale, genetically targeted optical control of neural activity. Nat. Neurosci. *8*, 1263–1268.
26. Petersen, C.C.H. (2007). The functional organization of the barrel cortex. Neuron *56*, 339–355.
27. Zhang, F., Wang, L.P., Brauner, M., Liewald, J.F., Kay, K., Watzke, N., Wood, P.G., Bamberg, E., Nagel, G., Gottschalk, A., and Deisseroth, K. (2007). Multimodal fast optical interrogation of neural circuitry. Nature *446*, 633–639.
28. Nathanson, J.L., Yanagawa, Y., Obata, K., and Callaway, E.M. (2009). Preferential labeling of inhibitory and excitatory cortical neurons by endogenous tropism of adeno-associated virus and lentivirus vectors. Neuroscience *161*, 441–450.
29. Tighilet, B., Hashikawa, T., and Jones, E.G. (1998). Cell- and lamina-specific expression and activity-dependent regulation of type II calcium/calmodulin-dependent protein kinase isoforms in monkey visual cortex. J. Neurosci. *18*, 2129–2146.
30. Aronoff, R., and Petersen, C.C.H. (2008). Layer, column and cell-type specific genetic manipulation in mouse barrel cortex. Front. Neurosci. *2*, 64–71.
31. Lefort, S., Tomm, C., Floyd Sarria, J.C., and Petersen, C.C.H. (2009). The excitatory neuronal network of the C2 barrel column in mouse primary somatosensory cortex. Neuron *61*, 301–316.
32. Matyas, F., Sreenivasan, V., Marbach, F., Wacongne, C., Barsy, B., Mateo, C., Aronoff, R., and Petersen, C.C.H. (2010). Motor control by sensory cortex. Science *330*, 1240–1243.
33. Tamamaki, N., Yanagawa, Y., Tomioka, R., Miyazaki, J., Obata, K., and Kaneko, T. (2003). Green fluorescent protein expression and colocalization with calretinin, parvalbumin, and somatostatin in the GAD67-GFP knock-in mouse. J. Comp. Neurol. *467*, 60–79.
34. Lampl, I., Reichova, I., and Ferster, D. (1999). Synchronous membrane potential fluctuations in neurons of the cat visual cortex. Neuron *22*, 361–374.
35. Crochet, S., Poulet, J.F.A., Kremer, Y., and Petersen, C.C.H. (2011). Synaptic mechanisms underlying sparse coding of active touch. Neuron *69*, 1160–1175.
36. Churchland, M.M., Yu, B.M., Cunningham, J.P., Sugrue, L.P., Cohen, M.R., Corrado, G.S., Newsome, W.T., Clark, A.M., Hosseini, P., Scott, B.B., et al. (2010). Stimulus onset quenches neural variability: A widespread cortical phenomenon. Nat. Neurosci. *13*, 369–378.
37. Waters, J., and Helmchen, F. (2006). Background synaptic activity is sparse in neocortex. J. Neurosci. *26*, 8267–8277.
38. Destexhe, A., Rudolph, M., and Paré, D. (2003). The high-conductance state of neocortical neurons in vivo. Nat. Rev. Neurosci. *4*, 739–751.
39. Kawaguchi, Y., and Kubota, Y. (1993). Correlation of physiological subgroupings of nonpyramidal cells with parvalbumin- and calbindinD28k-immunoreactive neurons in layer V of rat frontal cortex. J. Neurophysiol. *70*, 387–396.
40. Markram, H., Toledo-Rodriguez, M., Wang, Y., Gupta, A., Silberberg, G., and Wu, C. (2004). Interneurons of the neocortical inhibitory system. Nat. Rev. Neurosci. *5*, 793–807.
41. Burkhalter, A. (2008). Many specialists for suppressing cortical excitation. Front. Neurosci. *2*, 155–167.
42. Sakata, S., and Harris, K.D. (2009). Laminar structure of spontaneous and sensory-evoked population activity in auditory cortex. Neuron *64*, 404–418.
43. de Kock, C.P., and Sakmann, B. (2009). Spiking in primary somatosensory cortex during natural whisking in awake head-restrained rats is cell-type specific. Proc. Natl. Acad. Sci. USA *106*, 16446–16450.
44. O'Connor, D.H., Peron, S.P., Huber, D., and Svoboda, K. (2010). Neural activity in barrel cortex underlying vibrissa-based object localization in mice. Neuron *67*, 1048–1061.
45. Simons, D.J. (1978). Response properties of vibrissa units in rat SI somatosensory neocortex. J. Neurophysiol. *41*, 798–820.
46. Swadlow, H.A. (1989). Efferent neurons and suspected interneurons in S-1 vibrissa cortex of the awake rabbit: Receptive fields and axonal properties. J. Neurophysiol. *62*, 288–308.
47. Swadlow, H.A., and Gusev, A.G. (2002). Receptive-field construction in cortical inhibitory interneurons. Nat. Neurosci. *5*, 403–404.
48. Bruno, R.M., and Simons, D.J. (2002). Feedforward mechanisms of excitatory and inhibitory cortical receptive fields. J. Neurosci. *22*, 10966–10975.